Probing electron transfer mechanisms in *Shewanella oneidensis* MR-1 using a nanoelectrode platform and single-cell imaging

Xiaocheng Jiang[a,1], Jinsong Hu[a,1], Lisa A. Fitzgerald[b], Justin C. Biffinger[b], Ping Xie[a], Bradley R. Ringeisen[b,2], and Charles M. Lieber[a,c,2]

[a]Department of Chemistry and Chemical Biology, Harvard University, Cambridge, MA 02138; [b]Chemistry Division, US Naval Research Laboratory, 4555 Overlook Avenue, SW, Washington, DC 20375; and [c]School of Engineering and Applied Science, Harvard University, Cambridge, MA 02138

Contributed by Charles M. Lieber, August 5, 2010 (sent for review July 21, 2010)

Microbial fuel cells (MFCs) represent a promising approach for sustainable energy production as they generate electricity directly from metabolism of organic substrates without the need for catalysts. However, the mechanisms of electron transfer between microbes and electrodes, which could ultimately limit power extraction, remain controversial. Here we demonstrate optically transparent nanoelectrodes as a platform to investigate extracellular electron transfer in *Shewanella oneidensis* MR-1, where an array of nanoholes precludes or single window allows for direct microbe-electrode contacts. Following addition of cells, short-circuit current measurements showed similar amplitude and temporal response for both electrode configurations, while in situ optical imaging demonstrates that the measured currents were uncorrelated with the cell number on the electrodes. High-resolution imaging showed the presence of thin, 4- to 5-nm diameter filaments emanating from cell bodies, although these filaments do not appear correlated with current generation. Both types of electrodes yielded similar currents at longer times in dense cell layers and exhibited a rapid drop in current upon removal of diffusible mediators. Reintroduction of the original cell-free media yielded a rapid increase in current to ~80% of original level, whereas imaging showed that the positions of >70% of cells remained unchanged during solution exchange. Together, these measurements show that electron transfer occurs predominantly by mediated mechanism in this model system. Last, simultaneous measurements of current and cell positions showed that cell motility and electron transfer were inversely correlated. The ability to control and image cell/electrode interactions down to the single-cell level provide a powerful approach for advancing our fundamental understanding of MFCs.

bacteria | bioenergy | nanostructure | electron shuttles | nanowires

The capability of bacteria, such as *Shewanella* and *Geobacter*, to transfer electrons from metabolism of organic sources to electrodes without intervening catalysts serves as the basis for electricity production in microbial fuel cells (MFCs) (1–7). MFCs have been the focus of increasing interest for sustainable energy production because they feature long-term stability compared to other biological fuel cells (4), are able to operate at high efficiency (4), and are tolerant of a broad range of carbon feed stocks in waste water through renewable biomass (6, 7), although the low power density of MFCs has limited their applications to date (3–7).

Considerable progress has been made in improving power density through the optimization of fuel cell design (6, 7). Yet, a better understanding of charge transport at microbe/electrode interface is ultimately central to defining fundamental limits and possibly further improving power extraction in MFCs (3). Two limiting mechanisms have been proposed to explain the extracellular electron transfer in MFCs; these are (*i*) direct transfer of electrons from the outer cell membrane to the electrode (8, 9) and (*ii*) mediated electron transfer between the cell and electrode, where excreted soluble redox molecules serve as "electron shuttles" (10, 11). In addition, recent studies of filamentous pili growth from *Shewanella* and *Geobacter* cells report a third mechanism for extracellular electron transfer through biological nanowires (12, 13).

To address the fundamental electron transfer mechanisms operative in MFCs, we have developed and applied a general approach whereby (*i*) the physical contact between individual bacterial cells and electrodes is controlled using an insulating layer with designed nanoscale openings and (*ii*) simultaneous multiplexed measurements of current output from distinct electrode designs are made concurrently with single-cell resolution optical imaging of the electrode areas. An overview of our experimental approach (Fig. 1*A*) illustrates the transparent glass substrate with transparent electrode array enabling simultaneous current recording from multiple electrodes, and a polydimethylsiloxane (PDMS) chamber that allows for continuous or batch solution exchange and control of the ambient environment. A schematic of the design of individual electrodes used to control the interaction at the single-cell level (Fig. 1*B*) highlights the relative sizes of the nanohole and window openings in the insulating layer deposited over electrodes relative to individual bacteria such as *Shewanella*. The nanoholes are sufficiently small to preclude direct contact of the bacterial cell body to the active electrode surface, whereas multiple bacteria can contact the electrode in the case of the window.

Results and Discussion

We fabricated chips with 48 alternating nanohole/window transparent electrodes on glass slides using standard photolithography and electron-beam lithography techniques (see *Materials and Methods*). In short, photolithography and thermal evaporation were used to fabricate the array of transparent Ti/Au finger electrodes, and then plasma-enhanced chemical vapor deposition was used to deposit a silicon nitride passivation layer, and electron-beam lithography was used to define either nanoholes or windows at alternating electrodes in the array. We designed the openings such that nanoholes and window exposed the same electrode area, 12 μm^2, to solution. An optical micrograph (Fig. 1*C*) shows two adjacent finger electrodes separated by 25 μm with an array of nanoholes (*Left*) and single window (*Right*). Field-emission scanning electron microscopy (SEM) images further highlight the regular nanohole array (Fig. 1*D*) and rectangular window

Author contributions: X.J., J.H., L.A.F., J.C.B., P.X., B.R.R., and C.M.L. designed research; X.J., J.H., L.A.F., J.C.B., and P.X. performed research; X.J., J.H., L.A.F., J.C.B., P.X., B.R.R., and C.M.L. analyzed data; and X.J., J.H., B.R.R., and C.M.L. wrote the paper.

The authors declare no conflict of interest.

[1]X.J. and J.H. contributed equally to this work.

[2]To whom correspondence may be addressed. E-mail: bradley.ringeisen@nrl.navy.mil or cml@cmliris.harvard.edu.

This article contains supporting information online at www.pnas.org/lookup/suppl/doi:10.1073/pnas.1011699107/-/DCSupplemental.

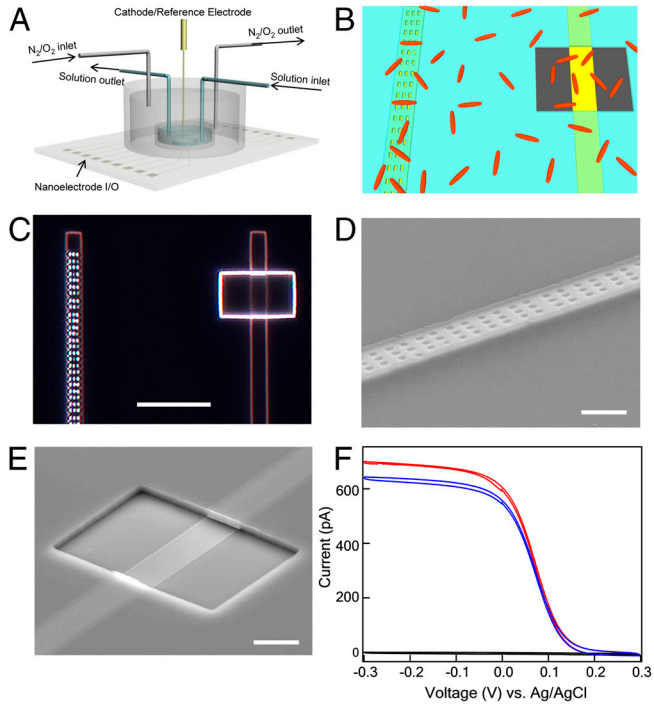

Fig. 1. Design and characterization of nanoelectrode chip. (*A*) Schematic of overall experimental design. Transparent electrode array is fabricated on 0.17-mm glass slide, enabling simultaneous current recording and optical imaging of cells on electrodes. A PDMS chamber is attached and sealed to the substrate, allowing for continuous or batch solution exchange, and control of the ambient environment by tuning the ratio of pure O_2 and N_2 gas sources using mass flow controllers. (*B*) Schematic of nanoelectrode design to control microbe/electrode interaction at the single-cell level. Nanoholes or window openings are defined in the silicon nitride insulating layer (blue) deposited over electrodes (yellow) to preclude or enable direct contact with microbes (red). The nanoholes and window are designed to expose the same electrode area to solution. Device fabrication and dimension details are specified in *Materials and Methods*. (*C*) Dark-field optical image of two adjacent finger electrodes separated by 25 μm with array of nanoholes (*Left*) and single window (*Right*). Scale bar, 10 μm. (*D* and *E*) Tilted-view SEM images of individual nanohole (*D*) and window (*E*) electrode. Scale bar, 2 μm. (*F*) Cyclic voltammetry measurement of adjacent finger electrodes with nanoholes (red), large window (blue), and full silicon nitride passivation (black) in 1-mM ferricyanide solution.

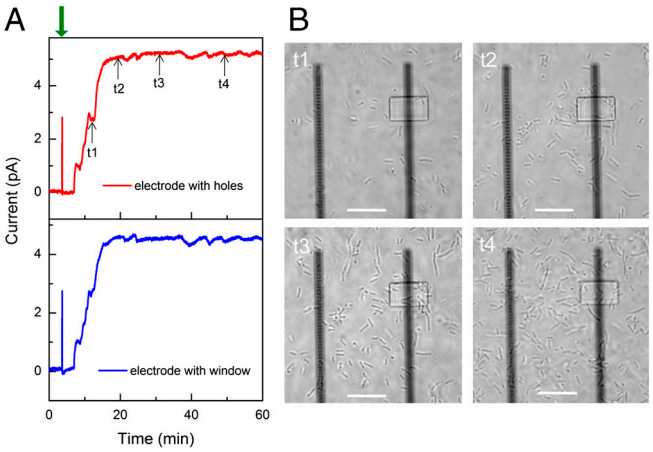

Fig. 2. Simultaneous current recording and optical imaging at early stage of cell landing. (*A*) Short-circuit current recording on electrodes with nanoholes (red) and large window (blue), respectively. Cell culture, electronics, and recording details are specified in *Materials and Methods*. In short, 0.5-mL cell culture was injected into measurement chamber at ~4 min (indicated by green arrow) after recording the stable baseline. The short-circuit current was recorded at an acquisition rate of 1 Hz with reference/cathode electrode (Ag/AgCl) grounded. (*B*) In situ phase-contrast images of MR-1 cells on adjacent electrodes with nanoholes (*Left*) and window (*Right*). The images were captured with an inverted phase-contrast microscope at 100× magnification, at 12 (t1), 20 (t2), 30 (t3), and 50 min (t4), respectively. Scale bar, 10 μm.

(Fig. 1*E*), where the relatively thick silicon nitride layer (ca. 400 nm) is clear in the tilted image of the latter.

In addition, we characterized the electrochemical behavior of the different electrodes by cyclic voltammetry in solution containing freely diffusing ferricyanide. All measurements in this work were carried out in a two-electrode configuration, with Ag/AgCl as both cathode and reference electrode. Recent redox protein electrochemistry studies using nanoelectrodes (14) verify that this approach is appropriate for our measurements because of the small short-circuit currents. Comparison of the data recorded from typical nanohole and window electrodes on the same chip (Fig. 1*F*) shows that the steady-state currents are comparable and thus consistent with similar active electrode areas and a diffusion limited process (14, 15). The current recorded from an adjacent electrode with full silicon nitride coating is <1% of the nanohole/window values (Fig. 1*F*), which shows that (*i*) only the defined openings contribute substantially to the measured currents and (*ii*) there is no cross-talk between adjacent electrodes.

We first used our experimental approach to characterize electron transfer from *Shewanella oneidensis* MR-1 (MR-1) cells at early times. Following addition of MR-1 cells (see *Materials and Methods*) to the chamber (Fig. 2*A*), the current recorded simultaneously from the adjacent nanohole (*Left*) and window (*Right*) electrodes began to increase within 5 min and reached a steady state of ~5 pA/electrode after 15 min despite the fact that the nanohole structure excludes direct cell membrane/electrode contact. The measured open circuit voltage at steady state was 0.45 V vs. Ag/AgCl for window and nanohole electrodes and is comparable to that reported previously for *Shewanella oneidensis* MFCs (16) after accounting for the difference in reference electrodes. Additional points can be gleaned from analysis of these data together with images of the distribution of MR-1 cells (Fig. 2*B*) recorded at the same time. Detailed comparison of current-time data shows that the onset and largest variations in current are *ca.* the same for the nanohole and window electrodes. Noise analysis before and after cell addition (Fig. S1) further demonstrates that observed similarities are not due to cross-talk between measured electrodes and are intrinsic to the electrochemical properties of MR-1 cells and solution. In addition, optical images recorded as the current reaches and maintains the steady-state value (Fig. 2*B*) demonstrate that (*i*) current generation initiates before cell membranes are in contact with the electrodes and (*ii*) the current does not increase after t2, although the cell number continues to increase on and in the area of both electrodes. Taken together, these experiments suggest that mediated electron transfer plays a dominant role at early times in our experiments and that MR-1 cells do not require direct contact with the electrode surface to generate a current.

We have carried out several experiments to further examine this conclusion. First, we find that the supernatant solution resulting from MR-1 culture cannot produce sustained short-circuit current (Fig. S2), indicating living MR-1 cells are required for persistent current output. Second, we have characterized the cell/electrode interface with SEM and atomic force microscopy (AFM) to address previous suggestions (12, 13) that biological nanowires might be important for extracellular electron transfer by MR-1. SEM images recorded from fixed samples (see *Materials and Methods*) show that MR-1 cell bodies are excluded from electrode contact by designed nanoholes (Fig. 3*A*), but are in intimate contact with the exposed electrode with the window (Fig. 3*B*). The SEM images also show that numerous cells are in close contact with the surrounding silicon nitride passivation layer for both

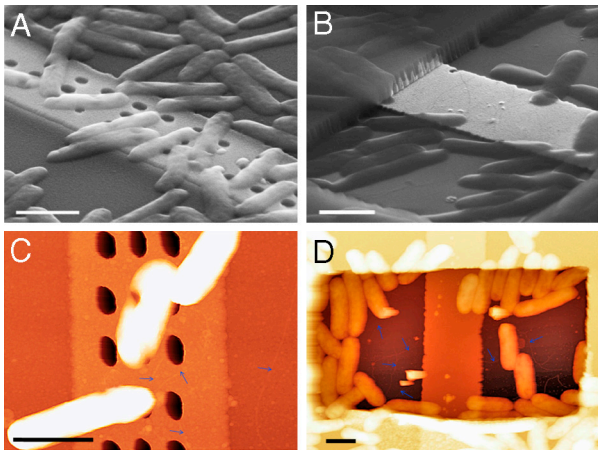

Fig. 3. Structural characterization of cell/electrode interface ~1 h after inoculation. Cell fixation and imaging details are specified in *Materials and Methods*. (*A* and *B*) SEM images of MR-1 cells on electrodes with nanoholes (*A*) and window (*B*). Scale bar, 1 μm. (*C* and *D*) AFM characterization of MR-1 cells on nanohole (*C*) and window (*D*) electrodes. The blue arrows indicate the thin filaments emanating from the cell bodies. Scale bar, 1 μm.

types of electrodes. Analysis of AFM images (Fig. 3 *C* and *D*) yielded similar overall results (e.g., cell bodies are excluded from electrode by nanoholes) and also demonstrated the presence of thin filaments with diameter of 4–5 nm (estimated from the height measurement) emanating from the cell bodies. The images also show that several filaments enter silicon nitride nanoholes, and for the window configuration, interact directly with exposed metal. However, it does not appear that these filaments are correlated with current generation under our experimental conditions given that (*i*) a similar current is observed for both nanohole and window electrodes before any cells are in contact with the electrodes (t1, Fig. 2) and (*ii*) as the number of cells on the electrodes increases (t2–t4, Fig. 2) there is no corresponding increase in current.

We have also investigated electron transfer at nanohole and window electrodes at longer times when multiple, continuous MR-1 cell layers or biofilms have formed on the electrode arrays. Short-circuit current measurements (Fig. 4*A*) exhibited a >70% decrease in current for both nanohole and window electrodes between 38 and 40 h, which we attribute to the depletion of electron donor (lactate) in the media. Injection of fresh lactate electron donor into the chamber (without changing the solution volume appreciably) yielded an immediate jump in current to a steady-state value of *ca.* 10 pA, thus confirming that the observed current output is associated with bacterial metabolism. This larger steady-state current in the dense cell layers compared with sparse cells at early times (Fig. 2) could be due to a higher local redox mediator concentration and/or depletion of residual oxygen in the medium. Although future experiments will be needed to address this point, we believe the key points from the experiments are the lack of correlation between current and local cell concentration near the electrodes and nearly identical current magnitude and temporal response from the distinct nanohole and window electrodes.

Two additional experiments were carried out using these dense cell layers to address the electron transfer mechanism. First, the supernatant in the measurement chamber was carefully removed and replaced with fresh, nitrogen purged medium after 42 h, which led to *ca.* 95% reduction in the short-circuit current at both the nanohole and window electrodes to steady-state values of 0.6 and 0.5 pA, respectively. Second and after an additional *ca.* 2 h of electrochemical cell operation, the original supernatant, which was centrifuged to remove planktonic cells, was exchanged with media in the measurement chamber, leading to an immediate

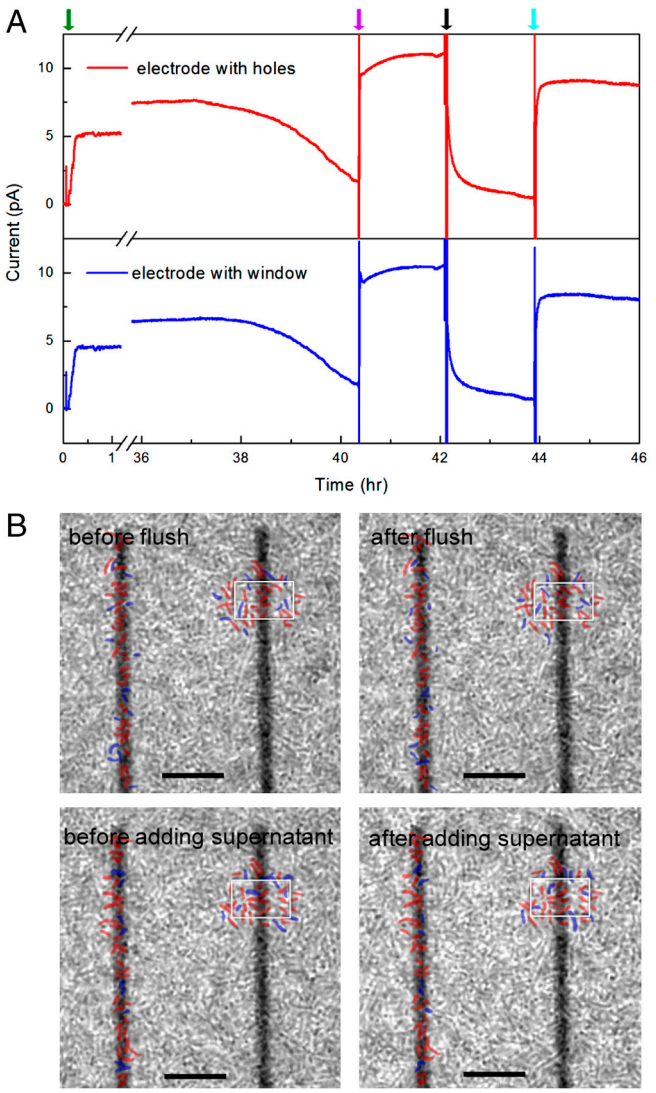

Fig. 4. Current and cell imaging measurements at long times with biofilm formation. (*A*) Long-term short-circuit current measurement on electrodes with nanoholes (red) and large window (blue), whereas the green, purple, black and cyan arrows indicate cell addition, lactate addition, flush by fresh MM, and supernatant addition, respectively. (*B*) Phase-contrast images of cells/electrode before, after flush and supernatant addition. Positions of cells near the nanohole (*Left*) and window (*Right*) electrodes that did not and did shift position during solution exchanges are marked in red and blue, respectively. The window is marked in white for clarity in each image; scale bars are 10 μm. Specific details of solution exchanges to/from the measurement chamber are as follows: 15 μL of 2 M sodium lactate [diluted from 60% Sodium DL-lactate solution (Sigma-Aldrich)] was directly injected into measurement chamber (containing ~1 mL solution), leading to final lactate concentration of ~30 mM with minimal dilution of other species. For the flush with fresh MM, the supernatant in measurement chamber was removed with a syringe, and then 1 mL nitrogen purged fresh MM (containing 30 mM lactate) was added to the chamber, where the addition of nitrogen purged fresh MM was repeated twice to ensure removal of mediators in the measurement chamber. The original supernatant, which was centrifuged at 3,000 rpm for 5 min to remove planktonic cells, was returned to the measurement chamber in the final exchange after removing the previous fresh MM by syringe. The original supernatant was diluted during solution exchange due to the incomplete removal of fresh media.

increase in short-circuit current to ~80% of original level recorded at both electrodes. The 20% difference in current amplitude could be due to a dilution effect (e.g., decrease in mediator concentration) because not all of the media could be removed during the exchange. In both exchange experiments, the current

changes were relatively rapid: 50% reduction in current after addition of fresh medium occurs within 5 min, and return to 50% of original current with addition of cell-free supernatant within 2 min. These results argue against a key role of pili in electron transfer in our system since it is difficult to rationalize why the first medium exchange might disrupt filaments (leading to reduced current), whereas the second medium exchange reconnects filament to electrodes on a even shorter time scale (and thus lead to an increase in the observed current).

The similar currents recorded after long time periods with the dense cell layers using nanohole electrodes (precluding direct cell contact) and window electrodes (allowing for direct contact) are best explained by a mediated electron transfer mechanism. The rapid current drop upon addition of fresh media and corresponding rapid recovery upon return of the original cell-free supernatant media support the requirement of diffusible redox mediators for electron transfer (11). However, it is possible to hypothesize in both cases that small pili (12, 13) are critical to electron transfer in the dense cell layers and that observed rapid current drop is due to disruption of cellular contacts during solution exchange (although as discussed above subsequent current increase on subsequent cell-free supernatant addition is difficult to reconcile with such a hypothesis). To address further this issue, single-cell-resolved images in the focal plane of electrode surfaces were obtained at each stage of the experiment shown in Fig. 4*A*. Notably, these images (Fig. 4*B*) demonstrate that <30% of MR-1 cells on the electrodes are perturbed; that is, their positions change after each solution exchange but were not removed from the surface. The majority of cells remain at the same positions, thus indicating that the observed changes in current output are unlikely to be due to structural changes in the cell/electrode interface.

Our results differ from solution exchange experiments with graphite felt (GF) anodes because in this previous work over 50% (vs. <5%) current was observed after removing the supernatant and planktonic cells (16, 17). We believe that the difference can be readily explained by the large surface area of GF, which although attractive for applications, makes it difficult to remove all solution species such as mediators from the system during exchange. Although the well-defined nanostructured transparent electrodes in our experiments do not maximize surface area as desired for applications, they do enable more detailed measurements for fundamental investigations.

More generally, the approach presented in this paper based on nanoelectrochemical measurements and simultaneous optical imaging can serve as a powerful platform for probing fundamental processes in MFCs and is thereby expected to advance our understanding of power extraction from MR-1 and other cellular systems. To exemplify this point we report early time current and imaging measurements made on chips in which the passivation was an organic polymer. The general increase in short-circuit current was similar to that discussed above. However, sharp current dips were observed during the early stages of cell deposition as shown in Fig. 5*A*. Notably, simultaneous in situ imaging (Fig. 5*B* and Movies S1, S2, and S3) demonstrates that each current dip correlated with an increase in the average cell speed: The average cell speeds immediately before (Movie S1), at the dip (Movie S2), and immediately after (Movie S3) were 5.5, 27, and 6.7 μm/s, respectively, whereas the short-circuit current level changed from 4.7 to 2.7 and back to 4.7 pA. The current change is independent of the cell number on the measured electrode and consistent with previous experimental results and mediated electron transfer mechanism. Ultimately, the amplitude of the current dips gradually decreased and the system finally reached a steady state with limited cell motion and stable current level comparable to the silicon nitride passivated chip electrode arrays. Similar behavior of *Shewanella* cells with dramatically increased motility was reported by Harris et al., but they attributed this phenomenon to increased extracellular electron transfer rates (18). Although

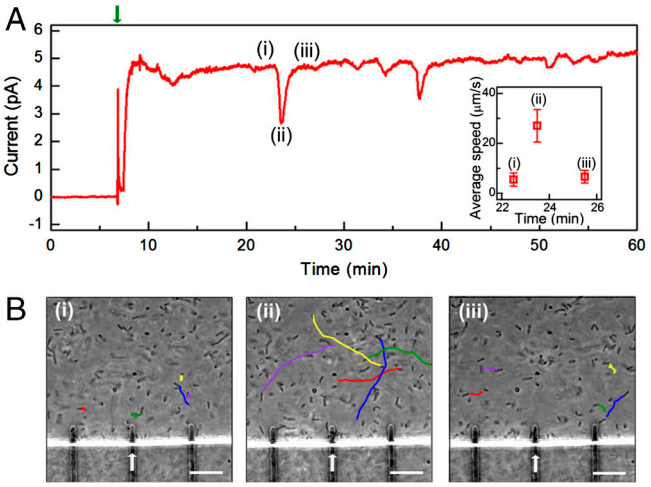

Fig. 5. Cell motility and current generation. (*A*) Short-circuit current recording on electrodes with organic polymer passivation rather than silicon nitride (Figs. 2–4). Device fabrication and measurement details are specified in *Materials and Methods*. The green arrow indicates the cell injection. Sharp current dips were observed during early stage of cell deposition. The average cell moving speed before (*i*), during (*ii*), and after (*iii*) the first spike dip at *ca.* 22 min was calculated from in situ microscopy videos (Movies S1, S2, and S3) and plotted as *Inset*. (*B*) Tracking trajectories for selected MR-1 cells during one second for period (*i*), (*ii*), and (*iii*). The trajectories were plotted based on real-time phase-contrast microscopy videos of MR-1 cells (Movies S1, S2, and S3) recorded at position of electrode used to record data in (*A*) (marked by white arrow). Scale bar, 10 μm.

an understanding of the mechanisms underlying this interesting behavior will require further study, the ability to record simultaneously current and cell positions shows that in our experiments motility and electron transfer are inversely correlated [contrasting the previous study (18)] and thus highlights the unique capabilities of our approach for probing MFCs down to the single-cell level.

Conclusions

We demonstrate a previously undescribed approach and unambiguous results addressing the mechanism of biological electron transfer in a model system *Shewanella oneidensis* MR-1. Nanostructured electrodes are designed and fabricated in which the presence or absence of cell body/electrode contact is physically controlled, so that the contribution from direct or mediated electron transfer could be distinguished. Because the electrodes are also optically transparent, we have been able to simultaneously record current output and microbe position/dynamics at the single-cell/microbe level. We find that at early times the current is uncorrelated with the number of cells on either type of electrode supporting a mediated electron transfer mechanism. A variety of experiments carried out after the formation of a biofilm also strongly argue for mediated electron transfer mechanism during steady-state MFC operation. Moreover, the ability to record simultaneously current and cell positions leads to the discovery that cell motility and electron transfer are inversely correlated in our system. Our current platform based on designed nanoelectrodes and in situ single-cell imaging is expected to advance significantly our fundamental knowledge of key factors affecting power extraction from MR-1 and other cellular systems.

Materials and Methods

Cell Culture. *Shewanella oneidensis* MR-1 were grown from −80 °C glycerol stock cultures by inoculating 50 mL of LB broth (Sigma-Aldrich) with gentle shaking (100 rpm) in air for approximately 48 h at 25 °C. The LB culture was then centrifuged at 3,000 rpm for 5 min to remove the supernatant. The cells were washed and redispersed with minimal media (MM) containing 30 mM sodium lactate. The formulation of MM was reported previously (19). The

redispersed culture was shaken (100 rpm) in air for 18 h at 25 °C before cell measurements.

Electrode Fabrication. Glass substrates (50 × 22 mm, 0.17 mm thick; VWR International) were cleaned in Piranha solution (3:1 concentrated sulfuric acid to 30% hydrogen peroxide) for 30 min, rinsed with deionized (DI) water (15 s), acetone (15 s), isopropanol (15 s), and dried in N_2 flow. A two-layer photoresist consisting of LOR3A and S1805 (Microchem) was sequentially deposited by spin-coating and baked for 5 min at 185 °C and 115 °C, respectively. The metal electrodes were defined by photolithography, followed by thermal evaporation of 2 nm Ti and 8 nm Au; 1 nm Ti was evaporated on top of Au as an adhesion layer in cases where Si_3N_4 was used for passivation. Each glass chip has 48 finger electrodes (2 μm wide, 25 μm spacing) defined at the chip center with fan out wiring to input/output points at the two ends of the chip. The finger electrodes were arranged in four groups of 12 parallel electrodes placed with their ends on the sides of a 500 μm × 500 μm square at the chip center. After liftoff, plasma-enhanced chemical vapor deposition was used to deposit ~400 nm Si_3N_4 over the entire chip. Poly(methyl methacrylate) was then coated on the chip, and e-beam lithography was used to define openings for access to the electrodes. At each addressable finger electrode either 150 holes (200 nm × 400 nm) or one window (6 μm × 10 μm) was defined to yield the same total exposed electrode area, ~12 μm^2; for each group of 12 parallel electrodes, alternating nanohole and window patterns were defined. Anisotropic reactive ion etching (50 sccm CHF_3, 30 sccm H_2, 3 mTorr, 75 W, 3 min) was used to remove Si_3N_4 in the patterned regions. Last, the electrodes were cleaned by 1 M sulfuric acid followed by UV ozone at 200 °C for 2 min. For SU-8 passivated chips, a ~2-μm-thick SU-8 layer was uniformly deposited, prebaked at 95 °C for 2 min, and then photolithography was used to define regions at the finger electrode tips. After postbaking at 95 °C for 2 min and development, the chip was hard-baked at 180 °C for 30 min. Finally, organic residues were removed from the electrodes by UV ozone treatment for 2 min at 200 °C.

Electrochemical Measurements. All measurements were carried out in a two-electrode configuration, with Ag/AgCl as both cathode and reference electrode. The current at the working electrode was detected using a current preamplifier (1211; DL Instruments, Inc.) with a gain of 10^9–10^{11} V/A. The amplified signals were digitized using a multichannel A/D converter (Digidata 1440 A; Molecular Devices). The Digidata 1440 A was also used to apply potentials during cyclic voltammetry measurements, with a typical sweep rate of 10 mV/s. The whole electrochemical cell was housed in a Faraday cage, yielding a noise level of <0.1 pA.

Cell Measurements and in Situ Optical Imaging. The short-circuit current was recorded at an acquisition rate of 1 Hz with reference/cathode electrode grounded. In situ optical imaging was carried out with an inverted phase-contrast microscope (IX71; Olympus Inc.) and 100X oil-immersion lens. The measurement atmosphere was precisely adjusted between strict anaerobic to microaerophilic conditions by tuning the ratio of pure O_2 and N_2 gas sources (0–10%) using mass flow controllers. As described previously, the largest current values were observed for a nonagitated, air-exposed condition (20, 21).

Cell Fixation and Imaging. After a fixed measurement time, supernatant and planktonic cells were carefully removed, and the chamber was refilled with 1 mL 4% cacodylate buffered glutaraldehyde solution (22) and fixed overnight at 4 °C. The fixing solution was then removed, and the chip was gently washed with DI water 3 times. Finally electrodes with cells were dehydrated in acetone for 5 min and dried in air. SEM and AFM analyses were carried out with Zeiss Supra55VP field-emission SEM and Digital Instruments Nanoscope IIIa MultiMode AFM, respectively. B.R.R. also acknowledges support from the Office of Naval Research Program Element 0601153N (NRL 6.1).

ACKNOWLEDGMENTS. We thank Dr. Fang Qian, Quan Qing, and Gene-Wei Li for helpful discussions. C.M.L. and B.R.R. acknowledge support of this work by the Air Force Office of Scientific Research. B.R.R. also acknowledges support from the Office of Naval Research Program Element 0601153N (NRL 6.1).

1. Fredrickson JK, et al. (2008) Towards environmental systems biology of *Shewanella*. *Nat Rev Microbiol* 6:592–603.
2. Bond DR, Holmes DE, Tender LM, Lovley DR (2002) Electrode-reducing microorganisms that harvest energy from marine sediments. *Science* 295:483–485.
3. Logan BE, Regan JM (2006) Electricity-producing bacterial communities in microbial fuel cells. *Trends Microbiol* 14:512–518.
4. Lovley DR (2006) Bug juice: Harvesting electricity with microorganisms. *Nat Rev Microbiol* 4:497–508.
5. Logan BE (2009) Exoelectrogenic bacteria that power microbial fuel cells. *Nat Rev Microbiol* 7:375–381.
6. Rabaey K, Verstraete W (2005) Microbial fuel cells: Novel biotechnology for energy generation. *Trends Biotechnol* 23:291–298.
7. He Z, Minteer SD, Angenent LT (2005) Electricity generation from artificial wastewater using an upflow microbial fuel cell. *Environ Sci Technol* 39:5262–5267.
8. Hartshorne RS, et al. (2009) Characterization of an electron conduit between bacteria and the extracellular environment. *Proc Natl Acad Sci USA* 106:22169–22174.
9. Chaudhuri SK, Lovley DR (2003) Electricity generation by direct oxidation of glucose in mediatorless microbial fuel cells. *Nat Biotechnol* 21:1229–1232.
10. Newman DK, Kolter R (2000) A role for excreted quinones in extracellular electron transfer. *Nature* 405:94–97.
11. Marsili E, et al. (2008) *Shewanella* secretes flavins that mediate extracellular electron transfer. *Proc Natl Acad Sci USA* 105:3968–3973.
12. Gorby YA, et al. (2006) Electrically conductive bacterial nanowires produced by *Shewanella oneidensis strain* MR-1 and other microorganisms. *Proc Natl Acad Sci USA* 103:11358–11363.
13. Reguera G, et al. (2005) Extracellular electron transfer *via* microbial nanowires. *Nature* 435:1098–1101.
14. Hoeben FJM, et al. (2008) Toward single-enzyme molecule electrochemistry: [NiFe]-hydrogenase protein film voltammetry at nanoelectrodes. *ACS Nano* 2:2497–2504.
15. Heinze J (1993) Ultramicroelectrodes in electrochemistry. *Angew Chem Int Edit* 32:1268–1288.
16. Ringeisen BR, et al. (2006) High power density from a miniature microbial fuel cell using *Shewanella oneidensis* DSP10. *Environ Sci Technol* 40:2629–2634.
17. Biffinger JC, Pietron J, Ray R, Little B, Ringeisen BR (2007) A biofilm enhanced miniature microbial fuel cell using *Shewanella oneidensis* DSP10 and oxygen reduction cathodes. *Biosens Bioelectron* 22:1672–1679.
18. Harris HW, et al. (2010) Electrokinesis is a microbial behavior that requires extracellular electron transport. *Proc Natl Acad Sci USA* 107:326–331.
19. Bretschger O, et al. (2007) Current production and metal oxide reduction by *Shewanella oneidensis* MR-1 wild type and mutants. *Appl Environ Microbiol* 73:7003–7012.
20. Biffinger JC, Byrd JN, Dudley BL, Ringeisen BR (2008) Oxygen exposure promotes fuel diversity for *Shewanella oneidensis* microbial fuel cells. *Biosens Bioelectron* 23:820–826.
21. Biffinger JC, et al. (2009) Simultaneous analysis of physiological and electrical output changes in an operating microbial fuel cell with *Shewanella oneidensis*. *Biotechnol Bioeng* 103:524–531.
22. Ray R, Little B, Wagner P, Hart K (1997) Environmental scanning electron microscopy investigations of biodeterioration. *Scanning* 19:98–103.